Hole and exciton energy levels in $InP/In_xGa_{1-x}P$ quantum dot molecules: Influence of geometry and magnetic field dependence

V. Mlinar,[1,*] M. Tadić,[1,2] and F. M. Peeters[1,†]
[1]*Departement Fysica, Universiteit Antwerpen, Groenenborgerlaan 171, B-2020 Antwerpen, Belgium*
[2]*Faculty of Electrical Engineering, University of Belgrade, P.O. Box 3554, 11120 Belgrade, Serbia*
(Received 22 December 2005; revised manuscript received 10 May 2006; published 20 June 2006)

Hole and exciton energy levels in vertically coupled double and triple InP/InGaP quantum dot molecules placed in an external magnetic field are analyzed. The size of the dots and the interdot distance in the quantum dot molecule (QDM) determine which one of the exciton quartets will have the lowest energy and determine also which one of the individual states in the quartet will be the ground state in the presence of an external magnetic field. Competition between confinement, quantum mechanical coupling, and strain influence the exciton diamagnetic shift in double and triple QDM. We found that the available experimental data [M. Hayne *et al.*, Phys. Rev. B **62**, 10324 (2000); Appl. Phys. Lett. **79**, 45 (2001)] are successfully described by *one* of the optically active exciton states of the lowest lying exciton quartet.

DOI: 10.1103/PhysRevB.73.235336 PACS number(s): 73.21.La, 78.67.Hc, 71.35.−y

I. INTRODUCTION

Recently, interest has moved towards coupling of low dimensional semiconductor structures to obtain new functional units.[1–6] The simplest example of such a unit is a pair of coupled quantum dots, a so-called quantum dot molecule (QDM). The Stransky-Krastanow growth process of quantum dot molecules is based on strain that surrounds a quantum dot in the lower lying layer which enforces the location of the next quantum dot on top of the first one.[7,8] Both electron and hole states in the quantum dot molecule were described in a similar way as bonding and antibonding states in a molecule. A shell structure of a QDM made of etched QDs, where a parabolic confinement potential is adopted, was analyzed in Refs. 9 and 10 using Hund-like rules. However, in the case of self-assembled QDMs such a simplified picture is not sufficient and the use of more complex models become necessary. The properties of self-assembled quantum dot molecules have been studied by several groups.[11–16] For example, in Refs. 12 and 13 the eight band $\mathbf{k}\cdot\mathbf{p}$ theory was employed to obtain the electronic structure of two vertically stacked InAs/GaAs quantum dots in the absence of any external field[12] and in the presence of an electric field.[13]

InP/InGaP QDs have attracted less attention, but they turned out to exhibit a lot of interesting fundamental physics and may also be important for potential applications, e.g., for red lasers.[20] From the fundamental point of view, it is interesting that with changing geometrical properties (size and shape) of the dot, one can control the position of the hole. For example, with increasing thickness of the dot it is possible to move the heavy hole out of the disk, and to create a type II system for the heavy holes.[17] In the case of a QDM the modified strain distribution in and around the dots directly affects the effective confinement potentials for the holes. Thus the interdot distance appears now as a new controllable parameter and a fundamental question about the spatial localization of holes and excitons in such a QDM arises. Furthermore, if an external magnetic field is introduced in such a system, additional confinement due to the magnetic field is present. Since we are dealing with dots having sizes of a few tens of nanometers this additional magnetic confinement significantly influences the electronic structure of the molecule in the magnetic field range of interest ($B \leq 50$ T). Recently, photoluminescence measurements on double and triple InP/InGaP QDMs in a magnetic field up to 50 T have been carried out.[18,19] In order to qualitatively explain those magnetophotoluminescence measurements, one has to employ a model that takes into account the strain field in and around the dots as well as the multiband mixing.

The InP/InGaP dot systems were previously studied theoretically: in Refs. 21 and 22 a single InP/InGaP QD was studied in the absence of any external fields, then an external magnetic field was applied in Refs. 17 and 23 and an extension to InP/InGaP QDM was presented in Refs. 15 and 16. In Ref. 15 the influence of strain on the exciton properties in triple QDM was discussed in the case a magnetic field was present. They assumed the dots to be disklike, strain was included through an isotropic model, and excitonic properties were calculated within the single-band effective mass approximation. This approach was extended in Ref. 16 where the continuum mechanical model was employed to model strain and the multiband effective mass approximation was used to calculate the electronic structure.

The aim of the present paper is to provide a consistent explanation of the spatial localization of holes and excitons in InP/InGaP QDMs, to investigate the behavior of the hole and exciton energy levels in the presence of an external magnetic field, and to compare the calculated exciton diamagnetic shift to the position of the photoluminescence peak from Refs. 18 and 19.

In the present paper we extend the model of Refs. 16 and 23 by including a perpendicular magnetic field for double and triple QDM. We model the dots forming the molecule by identical disks. The latter restriction can be justified as follows: (1) this is the most simple realistic model, (2) currently, there is no detailed knowledge available of the shape and alloy composition of the InP/InGaP single and stacked QDs that were used in the experiments, and (3) experiments on an ensemble of QDs average the finer details present in

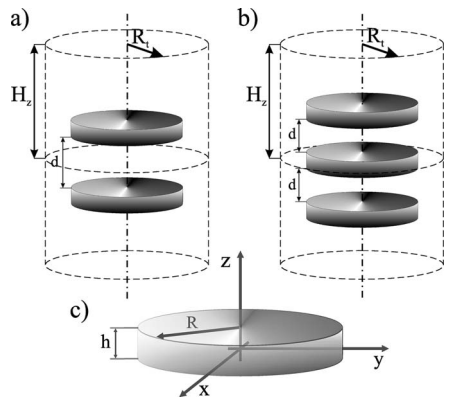

FIG. 1. The double (a) and triple InP/InGaP QDM (b) placed inside our simulation area (dashed lines), with radius R_t, and height $2H_z$. Dots are separated by an InGaP layer of thickness d. The system (a) and (b) are symmetric with respect to the $z=0$ plane. Dots are identical with radius R and thickness h where the Cartesian coordinates x, y, and z coincide with the [100], [010], and [001] crystallographic directions (c).

single QDs. The multiband theory of Pidgeon and Brown[24] is used which enables us to describe the magnetic field dependence of the absorption spectra. The effects due to strain are included through the continuum mechanical model and exciton energy states are computed by the exact-diagonalization approach, where electron-hole exchange interaction is neglected.

The paper is organized as follows. In Sec. II we give a short description of our theoretical approach, in Sec. III the influence of the dots size and interdot distance of the QDM on the ordering of hole and exciton energy levels is analyzed (Secs. III A and III B, respectively) and calculated exciton diamagnetic shifts for double and triple QDM are compared with the available experimental data (Sec. III C). Our results and conclusions are summarized in Sec. IV.

II. THE THEORETICAL APPROACH

Our models for the double- and triple-QDM consisting of self-assembled InP QD grown in the [001] direction are shown in Fig. 1. The dots are assumed to be flat disks, which is a good approximation for the large radius dots of Refs. 18 and 19 and we take them identical.

The Cartesian coordinates x, y, and z are taken along the [100], [010], and [001] crystallographic directions. In our theoretical approach, the shape of the dots is assumed to be cylindrical. R and h are radius and height of the dots, respectively [Fig. 1(c)], and d is the distance between the dots. The stack of two and three quantum dots is symmetric with respect to the $z=0$ plane where we assume equal distance between the dots and furthermore we neglect the wetting layer in our calculations.[25] The molecules are placed inside a large cylinder of radius R_t and height $2H_z$. The strain calculations as well as the electronic structure calculations are performed within this cylinder: (1) For the strain calculations we use the continuum mechanical model, where the displacements of the first-order finite elements are discretized onto a nonuniform grid. (2) The electron, hole, and exciton envelope functions are expanded within the cylinder.

Taking into account the symmetry of the molecule, the strain calculations can be restricted to the first octant. Details of the strain calculations can be found in Refs. 22, 16, and 26. In the present InP/InGaP quantum dot molecules only the valence subband mixing was explicitly included through the axial symmetric 6×6 multiband Hamiltonian, while the mixing between conduction and valence band could be omitted because of the large band gaps of the considered constituent materials. In the axial approximation the Hamiltonian is rotationally invariant around the z axis, which in our case leads to neglecting both the bulk in-plane warping of all valence bands and the shear strains and averaging the diagonal components of the strain tensor over the azimuthal angle. As a consequence of the axial symmetry, the z component of the total angular momentum can be introduced as a good quantum number,[27,28] $\mathbf{F}_z=f_z\hbar$. The z projection of the total angular momentum can be written as $F_z=J_z+L_z$, where J_z is the z component of the angular momentum of the band-edge Bloch function and L_z is the z component of the envelope angular momentum. Furthermore, if the quantum dots are symmetric with respect to the $z=0$ plane, which is fulfilled in our case, the parity of the wave function is a good quantum number. For example, the spinor of the even valence-band state has the form[22]

$$F_{f_z}^{+}=[F_{hh}^{+},F_{lh}^{-},F_{so}^{-},F_{hh}^{-},F_{lh}^{+},F_{so}^{+}]. \tag{1}$$

Here *hh* denotes the heavy hole, *lh* the light hole, and *so* the spin-orbit split-off band. The ± sign in the superscript of the envelope functions denotes the parity of the envelope function [+ (−) for even (odd) envelope function]. The hole states for a given quantum number f_z are denoted by $nX_{f_z}^{par}$ (Ref. 28), where n is the label of the state for given f_z, X denotes the minimum value of $|l|$ in the chosen basis set for the valence band states, and *par* represents the parity of the state [+ (−) for even (odd) parity]. The exciton energy states are computed using the exact-diagonalization approach, where the electron-hole exchange interaction is neglected. The latter interaction is not important in type II systems. The exciton wave function is expanded into pairs formed by the zone-center single-particle electron and hole wave functions,

$$\Psi_{exc}(\mathbf{r}_e,\mathbf{r}_h)=\sum_{s,j_h}F_{s,j_h}(\mathbf{r}_e,\mathbf{r}_h)|s\rangle|j_h\rangle, \tag{2}$$

where s denotes the electron spin, j_h is the magnetic quantum number of the holes, and F_{s,j_h} is the envelope function of the exciton. The z component of the total angular momentum ($F_{zexc}=F_{ze}-F_{zh}$) is a good quantum number for the exciton. The parity of the exciton can be introduced as a good quantum number.[16] As a consequence, the exciton states can be classified by electron spin, z projection of angular momentum of the exciton, and the parity. The exciton states are denoted as $nX_{f_{exc}}^{\sigma_{exc}}$. Since the electron-hole exchange interaction is neglected in our calculations, each exciton level is fourfold degenerate in the absence of a magnetic field[23] because of spin degeneracy and Kramers degeneracy of the holes. Examples of these quartets are

$$Q_1^+ = \left[\boxed{S^+_{-1\uparrow}}_{(x,y)} \quad S^-_{+2\uparrow} \quad \boxed{S^-_{+1\downarrow}}_{(x,y)} \quad S^+_{-2\downarrow} \right], \tag{3a}$$

$$Q_2^- = \left[\boxed{S^-_{0\uparrow}}_{(z)} \quad \boxed{S^+_{+1\uparrow}}_{(x,y)} \quad \boxed{S^-_{-1\downarrow}}_{(x,y)} \quad \boxed{S^+_{0\downarrow}}_{(z)} \right], \tag{3b}$$

where the optical active states in the quartet are indicated by a box and the subscripts (x,y) and z for in-plane and z polarized light, respectively. Recombination of an exciton depends on the polarization sensitive selection rules for the zone center wave functions and the selection rules resulting from the conservation of the envelope angular momentum. The oscillator strength is used as a figure of merit for the recombination of an exciton [Eq. (4)]

$$f = \frac{2}{m_0 E_{exc}} |M_{exc}|^2, \tag{4}$$

where E_{exc} denotes the recombination energy, m_0 is the free electron mass, and M_{exc} is the transition matrix element given by

$$M_{exc} = \int_{\mathbf{r}_e \mathbf{r}_h} \boldsymbol{\epsilon} \mathbf{p}_h \tilde{\Psi}_{exc} d\mathbf{r}_e d\mathbf{r}_h, \tag{5}$$

where $\boldsymbol{\epsilon}$ denotes the polarization vector, Ψ_{exc} is the wave function composed of valence band electron envelope functions and the conjugate complex of the conduction band electron envelope functions, $\mathbf{p}_h$ acts only on the valence band zone center periodic parts of the Bloch functions, and the integration is performed over electron and hole coordinates. Details of the calculations of the electron, hole, and exciton energy spectra were already given elsewhere.[16,22] In the case of a magnetic field, the vector potential should be incorporated into the $\mathbf{k}$ operator of the Hamiltonian.[29,30] The magnetic field also gives rise to a Zeeman energy term which removes Kramers degeneracy which further leads to lifting of the degeneracy arranged by exciton quartets.

To show more clearly the exciton magnetic field dependence, we analyze the exciton diamagnetic shift, defined as

$$\Delta E_{exc} = E_{exc}(B) - E_{exc}(B = 0T). \tag{6}$$

III. NUMERICAL RESULTS AND DISCUSSION

In our numerical calculations, radius and height of the InP quantum dots in the double and triple quantum dot molecules are varied in the range 6–10 nm and 2–4 nm, respectively. The distance between the dots is varied over $d=1.5$–8 nm. The large cylindrical simulation region was taken with dimensions $R_t=30$ nm and $2H_z=100$ nm (see Fig. 1). For the strain calculations we took a grid with 65 vertices along ρ, 101 vertices along the z direction, and 33 vertices along the ϕ direction. The electron and hole wave functions are expanded into a basis consisting of 10 Bessel and 50 sin or cos functions. The exciton states are computed for both electron spins and values of f_{exc} in the range $-2 < f_{exc} < 2$, where only some of the exciton states are found to be optically active. The material parameters for $InP/In_{0.49}Ga_{0.51}P$ are listed in Table I of Ref. 22. For the conduction-band effective masses in InP and InGaP we used $0.0795m_0$ and $0.092m_0$, respectively (Ref. 31), where m_0 denotes the free electron mass.

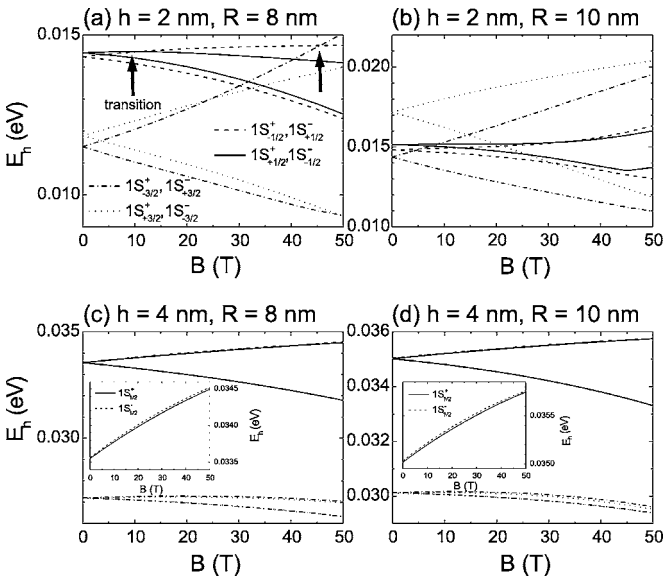

FIG. 2. Hole energy levels as a function of the magnetic field for dot radii $R=8$ nm and heights $h=2$ nm (a), dot radii $R=10$ nm and heights $h=2$ nm (b), dot radii $R=8$ nm and heights $h=4$ nm (c), and dot radii $R=10$ nm and heights $h=4$ nm (d). Interdot distance is 1.5 nm. Black arrows indicate the transition fields of the hole ground state.

A. DQDM hole states: Influence of geometry and magnetic field dependence

Here, we discuss the influence of the size (height and radius) of the dots forming the molecule, the interdot distance, and the magnetic field on the hole energy levels of a double QDM. To simplify our model we consider two vertically aligned identical quantum dots forming a QDM. The electron wave function is symmetrically distributed over the dots, and its qualitative behavior is not significantly influenced by interdot distance and the dots size.[15,16] The hole energy levels as a function of the magnetic field for two interdot distances $d=1.5$ and 5 nm are shown in Figs. 2 and 3, respectively.

Two values of the dot radius, 8 and 10 nm, and dots height, 2 and 4 nm, are considered in Fig. 2. Notice that the size of the dots in the molecule influences the ordering of the hole energy levels. For the dots radius $R=8$ nm and height $h=2$ nm the hole ground state is $1S^+_{1/2}$, but when we increase the radius to 10 nm the hole ground state becomes $1S^+_{3/2}$. If the dots height is increased as well (to 4 nm), the hole ground state becomes $1S^-_{1/2}$ [see inset of Fig. 2(d)]. Decreasing the dot radius to 8 nm, but keeping the height unchanged ($h=4$ nm) does not change the character of the hole ground state. Because the hole energy levels $1S^{\pm}_{\pm 1/2}$ and $1S^{\mp}_{\mp 1/2}$ and $1S^{\pm}_{\pm 3/2}$ and$1S^{\mp}_{\mp 3/2}$ for dot height $h=4$ nm and for both dot radius $R=8$ and 10 nm are nearly degenerate we show in the insets of Figs. 2(c) and 2(d) the lowest hole energy levels as they vary with magnetic field. Small interdot distance pre-

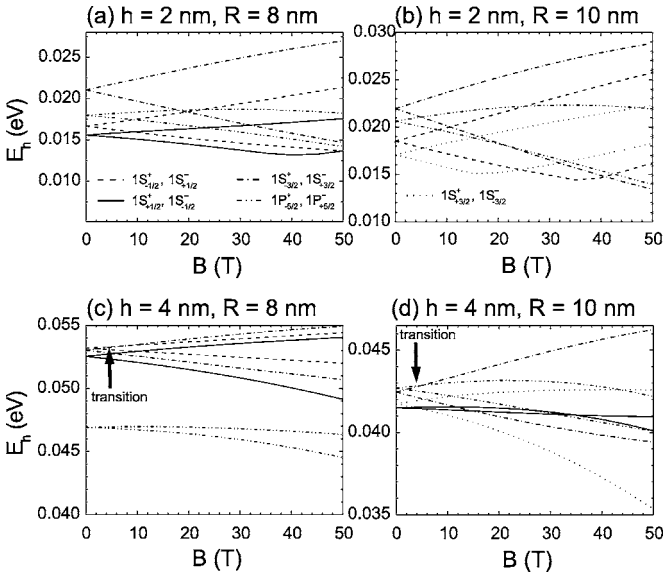

FIG. 3. The same as Fig. 2 but now for an interdot distance of 5 nm.

vents the hole to sit between the dots which leaves us three possibilities. The hole can sit above and below the stack, inside the dots, or outside the dots in the radial direction. The location of the holes is determined by the strain field as well as by the Coulomb interaction with the electron whose wave function is symmetrically distributed over the dots. Location of the hole ground state is shown in Fig. 4.

Only for a dot radius $R=10$ nm and height $h=2$ nm we find that the hole ground state is localized in the dots and it is heavy-hole-like, in all other considered cases the hole sits above and below the stack and it is light-hole-like. Terms heavy-hole-like and light-hole-like are used just to stress the dominant contribution of one of the three bands (heavy hole, light hole, spin-orbit band) to the hole ground state.

Presence of a magnetic field removes Kramers degeneracy between even and odd parity hole states (Fig. 2). For example, hole states $1S^{+}_{1/2}$ and $1S^{-}_{-1/2}$ are degenerate in the absence of a magnetic field, but lifting the degeneracy and

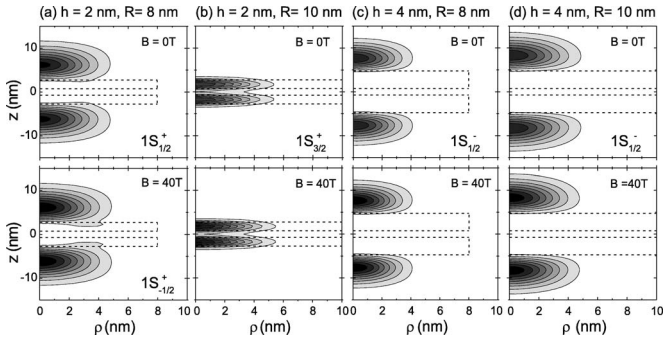

FIG. 4. Double QDM: the contour plot of the hole ground state probability density for $B=0$ and 40 T, for dot radii $R=8$ nm and heights $h=2$ nm (a), dot radii $R=10$ nm and heights $h=2$ nm (b), dot radii $R=8$ nm and heights $h=4$ nm (c), and dot radii $R=10$ nm and heights $h=4$ nm (d). Interdot distance is 1.5 nm. The dotted lines outline the position of the dots.

splitting of those two energy levels come forward as a consequence of an applied magnetic field. Increasing the dot radius leads to a stronger influence of the magnetic field through magnetic field induced band mixing and Zeeman splitting. Furthermore, if one follows the behavior of the hole ground state energy as a function of the magnetic field (see Fig. 2), one can see that the character of the hole ground state changes in the case of a dot radius $R=8$ nm and height $h=2$ nm. The first hole ground state transition occurs for $B=10$ T where the hole ground state transitions from $1S^{+}_{1/2}$ to $1S^{+}_{-1/2}$, and then at $B=45$ T, the hole ground state changes to $1S^{+}_{-3/2}$. Using the simplified but useful heavy- and light-hole-like states picture, one can see that the transition at 10 T keeps the light-hole-like ground state, but changes only the z-projection of the total angular momentum (from $1S^{+}_{1/2}$ to $1S^{+}_{-1/2}$), and that the hole ground state transition at $B\approx 45$ T is a transition from the light-hole-like ground state to the heavy-hole-like ground state (from $1S^{+}_{-1/2}$ to $1S^{+}_{-3/2}$). The reason for the second transition can be found in the stronger effect of the magnetic field on the heavy-hole-like states. Note that the in-plane heavy-hole mass is lighter than the in-plane light-hole mass, and the lighter the in-plane mass is, the larger is the magnetic field energy. Increasing the dot radius to $R=10$ nm, a transition from the state $1S^{+}_{3/2}$ to $1S^{+}_{-3/2}$ will occur for a magnetic field larger than 50 T [see Fig. 2(b)]. In contrast, when increasing the dot height no hole ground state transition is found as a function of the magnetic field.

For interdot distance $d=5$ nm, the two dots in the molecule are mainly coupled by the strain field since strain decays by a power law, and electron and hole wave functions decay exponentially. Hole energy levels as a function of the magnetic field are shown in Fig. 3. As in the case of interdot distance $d=1.5$ nm, quantum dots geometrical properties influence the reordering of the hole states. In the absence of a magnetic field, for a dot height of 2 nm, the hole ground state is $1S^{-}_{3/2}$ for both dots radius $R=8$ and 10 nm. But for a larger dots height of $h=4$ nm the hole ground state is $1S^{-}_{1/2}$ when the dots radius is $R=8$ nm and $1S^{-}_{5/2}$ when the dots radius is increased to $R=10$ nm. Compared to the case of interdot distance $d=1.5$ nm where the hole could not sit between the dots, for this interdot distance $d=5$ nm there is also a possibility for the hole to be localized between the dots. The corresponding hole ground state probability densities are shown in Fig. 5.

For the dot height 2 nm, the hole ground state is heavy-hole-like and it is mainly located inside the dots, where for the dot radius $R=8$ nm, there is a contribution of the light-hole bands in between the two dots. However, for a dot height of $h=4$ nm, the hole sits in between the dots (see Fig. 5) for both dots radius $R=8$ and 10 nm and it is light-hole-like.

Compared to the case of interdot distance $d=1.5$ nm, where hole ground state transitions were observed as a function of the magnetic field for dot heights of $h=2$ nm, magnetic field induced hole ground state transitions for the case $d=5$ nm are found for a dot height of $h=4$ nm. For both values of the dot radius $R=8$ and 10 nm, the transition occurs at $B\approx 5$ T. For dot radius $R=8$ nm, a transition from the state $1S^{-}_{1/2}$ to $1S^{-}_{3/2}$ is observed, while for dot radius R

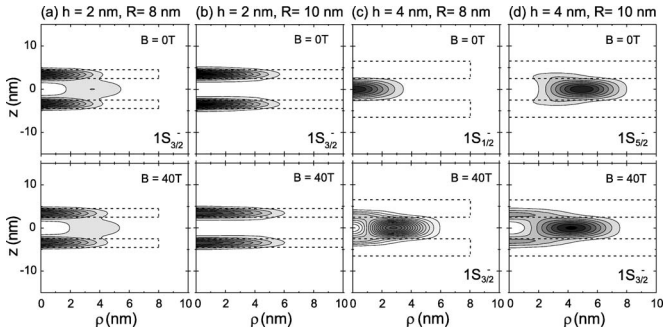

FIG. 5. The same as Fig. 4 but now for interdot distance of 5 nm.

$=10$ nm, a transition from the state $1S_{5/2}^{-}$ to $1S_{3/2}^{-}$ is observed—in both cases from the light-hole-like ground state to the heavy-hole-like ground state. One can see that whenever the hole ground state for $B=0$ T is heavy-hole-like a magnetic field will not induce any transition of the hole ground state because of the larger shift of the heavy-hole-like states in a magnetic field.

Let us also briefly discuss the kinks in the hole energy levels as a function of a magnetic field [for example, see the hole state $1S_{-1/2}^{-}$ in Fig. 2(b) or the hole state $1S_{-3/2}^{-}$ in Fig. 3(b)]. We have already discussed crossings between the lowest lying hole states of either different parity or z-projection of total angular momentum (Figs. 2 and 3). Since the hole states are classified with respect to their z component of total angular momentum, their parity and their principal quantum number (see discussion in Sec. II), crossings between the states of the same z component of total angular momentum and the same parity are forbidden.[27,28] Thus kinks in the hole energy level as a function of the magnetic field are a consequence of the anticrossing of that hole state with the hole state of the same parity and the same z component of total angular momentum but different principal quantum number.[22,27,28]

B. Double QDM exciton states: Influence of geometry and magnetic field dependence

We investigate now the lowest exciton levels for a double QDM as a function of the magnetic field. For interdot distances $d=3$ and 8 nm (see Fig. 6) we take the dot height 2 nm and vary the dot radii in the range 6–10 nm. For the case with interdot distance 3 nm [see Fig. 6(a)] and dot radii 6 and 8 nm the lowest exciton levels belong to the Q_1^- exciton quartet, and all individual states in that quartet are optically inactive [inset of Fig. 6(a) for $R=6$ and 8 nm] and the first optically active quartet is Q_2^- [Fig. 6(a) for $R=6$ and 8 nm].

For dot radius $R=10$ nm the lowest exciton levels belong to the Q_1^- exciton quartet as well, but the lowest optically active exciton levels belong to the Q_1^+ exciton quartet [Fig. 6(a) and inset, for $R=10$ nm]. The exciton ground state is $S_{-2\downarrow}^{+}$. Thus for a fixed interdot distance and dot height, the size of the dots in the lateral direction determines which exciton quartet will be the ground state. Presence of a magnetic field lifts the degeneracy and the fourfold degenerate

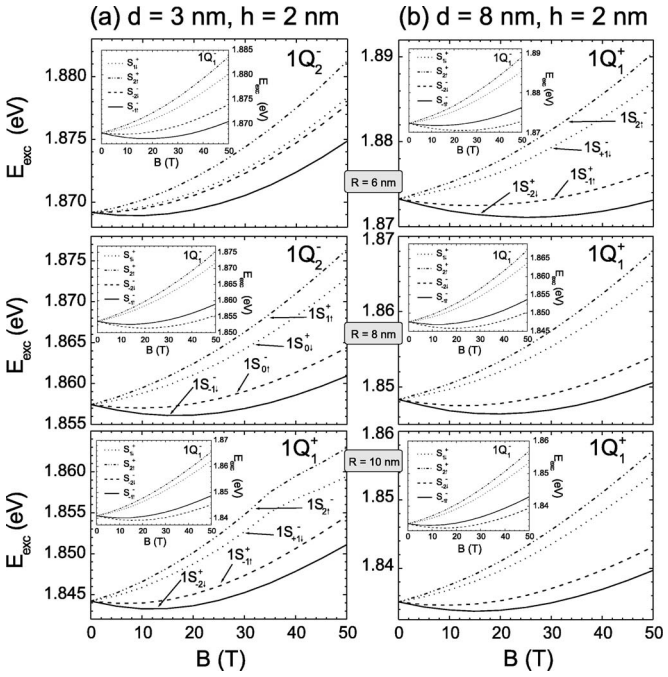

FIG. 6. Splitting of the lowest lying optically active exciton quartet into four branches as a function of magnetic field for a double InP/InGaP QDM. Dot radius is varied from 6 to 10 nm, with fixed thickness of the dot $h=2$ nm and fixed interdot distance $d=3$ nm (a) and interdot distance $d=8$ nm (b). The insets depict the ground state quartet, but where all the individual states are optically inactive.

exciton energy splits into four levels. Some of those individual states are optically active (bright exciton) and others not (dark exciton).

Exciton probability densities for interdot distance $d=3$ nm and for three different values of the dot radius $R=6$, 8, and 10 nm are shown in Figs. 7(a)–7(c), respectively. Only the probability densities of the lowest lying optical active exciton state belonging to the first optical active exciton quartet for $B=0$, 20, and 40 T are plotted. For example, for the case of the dot radius $R=8$ nm, the exciton wave function of the state $S_{-1\downarrow}^{-}$ of the Q_2^- quartet is shown in Fig. 7(b). One can see that increasing the dot radius from $R=6$ to 8 nm tends to place the exciton more inside the dots, where for $R=10$ nm, the exciton is completely localized inside the dots. Presence of the magnetic field does not lead to a redistribution of the exciton wave function, but just enhances the electron-hole overlap. With increasing interdot distance to $d=8$ nm, changing the dot radius does not influence the exciton ground state quartet which is always Q_1^- [insets of Fig. 6(b)] and the first optically active quartet is Q_1^+ [Fig. 6(b)].

Let us also briefly discuss the optical activity of the individual states belonging to the lowest exciton quartets. For example, for the dot radius $R=8$ nm, the states of the Q_2^- exciton quartet are split into a pair of two branches: lower lying $S_{-1\downarrow}^{-}$ and $S_{0\downarrow}^{+}$ and upper lying $S_{+1\uparrow}^{+}$ and $S_{0\uparrow}^{-}$. In Fig. 8(a), oscillator strength for exciton recombination as a function of the magnetic field is shown. All states are optically active, $S_{+1\uparrow}^{+}$, $S_{-1\downarrow}^{-}$ for x,y polarization of the light, and $S_{0\downarrow}^{+}$ and $S_{0\uparrow}^{-}$ for z polarization.

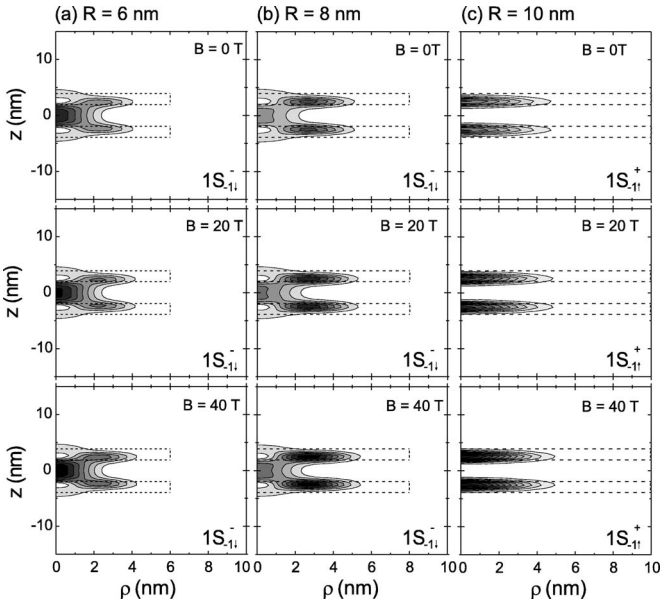

FIG. 7. The probability density of the lowest lying optical active exciton state belonging to the first optical active exciton quartet for $B=0$, 20, and 40 T in a double InP/InGaP QDM. The exciton wave functions for dot radius $R=6$ nm (a), $R=8$ nm (b), and $R=10$ nm (c) are shown. Dot thickness is fixed to $h=2$ nm and the interdot distance to $d=3$ nm.

However, optical activity for x and y polarization is an order of magnitude smaller than for z polarization [see Fig. 8(a)]. Next, as an example of the optical activity for the Q_1^+ quartet, oscillator strength for exciton recombination as a function of the magnetic field for the exciton Q_1^+ quartet for $d=3$ nm and dot radius $R=10$ nm is calculated. Only two individual states, $S_{-1\uparrow}^+$, $S_{1\downarrow}^-$, of the exciton Q_1^+ quartet are optically active, and only for x,y polarization. The oscillator strength as a function of the magnetic field is shown in Fig. 8(b) which is two orders of magnitude larger than for the $1Q_2^-$ state of Fig. 8(a). There is no optical activity for z polarization.

For completeness, influence of the variation of interdot distance, dots, height, and radius on the double QDM magnetoexciton states is investigated. Results of our calculations are shown in Fig. 9(a) for interdot distance $d=1.5$ nm and in Fig. 9(b) for interdot distance $d=5$ nm.

It can be seen from Fig. 9(a) (interdot distance $d=1.5$ nm) that the size of the dots in the vertical direction

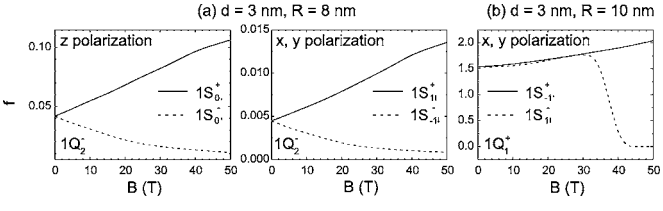

FIG. 8. Oscillator strength for exciton recombination as a function of the magnetic field for the exciton quartet Q_2^- with the states $S_{+1\uparrow}^+$, $S_{-1\downarrow}^-$ for x,y polarization, and $S_{0\downarrow}^+$ and $S_{0\uparrow}^-$ for z polarization (a) and for the exciton quartet Q_1^+ for the states $S_{-1\uparrow}^+$,$S_{1\downarrow}^-$ for x,y polarization (b).

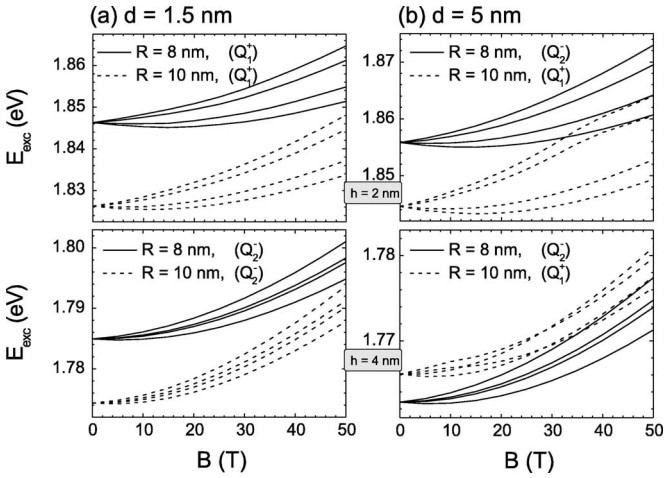

FIG. 9. Splitting of the lowest lying optically active exciton quartet as a function of magnetic field in a double InP/InGaP QDM for interdot distance $d=1.5$ nm (a) and $d=5$ nm (b). Exciton levels for two values of the dot radius $R=8$ and 10 nm, and two values of the dot height $h=2$ and 4 nm are plotted.

determines which exciton quartet will be the ground state. However, when increasing the interdot distance to $d=5$ nm [Fig. 9(b)], the ordering of the exciton quartets depends on the dot size in the lateral direction. Note that for the bright exciton ground states no ground state transitions were found as a function of the magnetic field and the energetically lowest exciton quartet is only determined by the dot size and the interdot distance (Figs. 6 and 9). In Ref. 16 the variation of the exciton energies with interdot distance was analyzed for fixed value of the dot radius ($R=8$ nm) in the absence of a magnetic field. The effect of the coupling between the dots was investigated, but there was no comparison with the effect due to the lateral confinement in the dots, which, as is shown in Figs. 6 and 9, cannot be neglected. It is also worth mentioning that for interdot distance $d=5$ nm and dot height $h=4$ nm, the ground state exciton quartet for $R=8$ nm is lower in energy than the exciton quartet for $R=10$ nm. This is a direct consequence of the hole location [see Fig. 5(d)] and the weaker Coulomb interaction than in the case for a dot radius of $R=8$ nm [see Fig. 5(c)].

C. Comparison with experiment

We compare our theoretical results with experimental data from Refs. 18 and 19 for triple and double quantum dot molecules. It should be pointed out that the shape and size of the dots are not known very accurately. Strain and alloy fluctuations will affect, for example, the localization of the charged particles and may lead to an asymmetric distribution of the particles along the z direction. Transmission electron microscopy showed that dots in the triple QDM analyzed in Ref. 18 were most likely lens or disk shaped with approximately 16 nm diameter and 2 nm height, and that the dots in the stacked-layer samples were vertically aligned. Measurements on the samples with interdot distances of $d=2$, 4, and 8 nm (samples D, C, B in Ref. 18, respectively) will be compared with our theoretical results. For the case of the

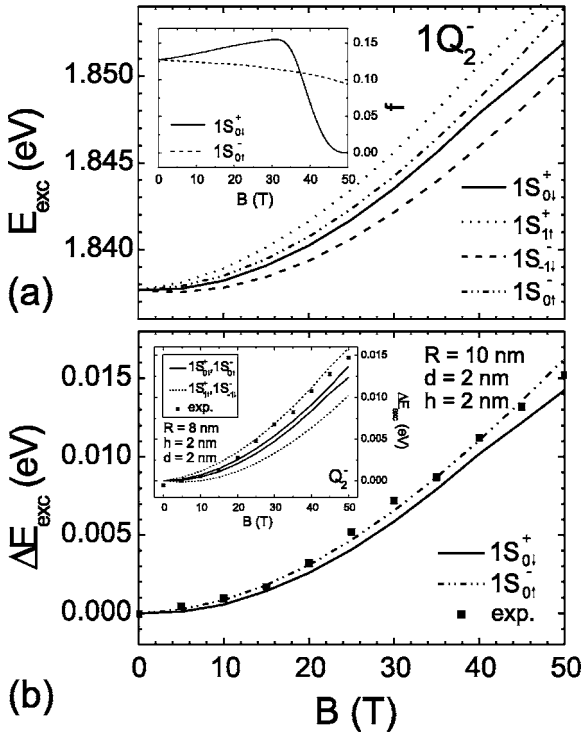

FIG. 10. (a) The ground state exciton quartet for the triple QDM. Dot radius $R=10$ nm, thickness $h=2$ nm, and interdot distance $d=2$ nm. In the inset of (a) the oscillator strength of the optical active states for z-light polarization are shown. (b) Exciton diamagnetic shift as a function of magnetic field for the optical active exciton states compared to the experimental results (symbols) of Ref. 18. In the inset of (b) comparison of optically active exciton states where nominal experimental parameters are used ($R=8$ nm, $h=2$ nm, $d=2$ nm) with the experimental results.

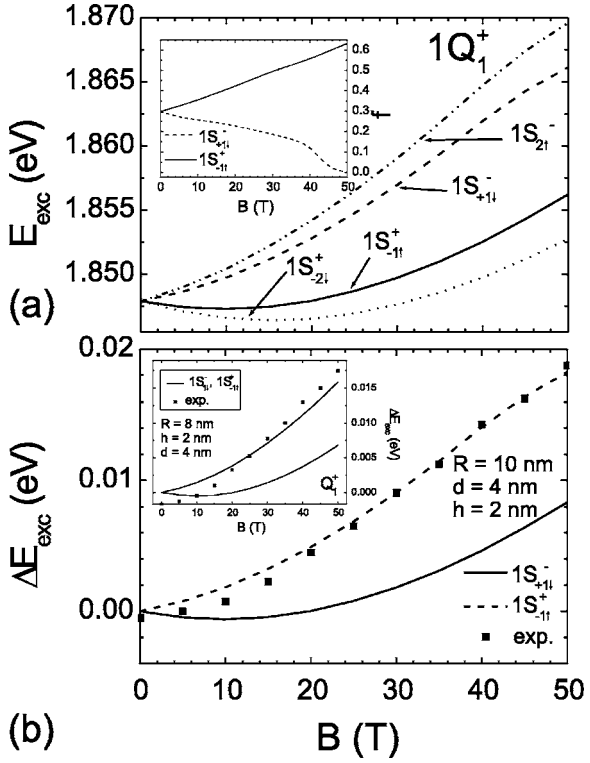

FIG. 11. The same as Fig. 10 but now for interdot distance $d=4$ nm. Inset of (a) is now for the x,y light polarization, and in inset of (b) calculated exciton diamagnetic shift for experimentally given size of the dots ($R=8$ nm, $h=2$ nm, $d=4$ nm) is compared with experimental data.

double QDM, QDs were taken as flat with diameter 16 nm, and height 2 nm.[19] Further, authors from Ref. 19 analyzed double QDM with different size dots in the stack, but we compare our theoretical results with the measurements on the sample with the same amount of InP (sample A in Ref. 19).

Our theoretical findings for the exciton diamagnetic shift for triple QDM are compared with the experimental results of the position of the photoluminescence peak (squares). The results are shown in Figs. 10–12, and are in good agreement with the experiment. Experimental data are always well-described by the lowest lying exciton quartet, but not always with the lowest optically active individual exciton state belonging to that quartet. Note that the main goal of this comparison is not to fit our results to the experimental curves, but to explain the experimental results in the framework of the applied theory. Thus we did not fit any effective mass parameter. Growth details of these stacked QDs were given in Ref. 32 and it is well-known that lateral dot size fluctuation and fluctuation in the total height of the dot stack (height of the dots + interdot distances) determine the PL linewidth and that the influence of fluctuations in the height of the dots reduces once they become coupled in the stack. Furthermore, the smaller the interdot distance the smaller the influence of height fluctuations (Refs. 18 and 32). How do we approach the problem? We choose a QDM which we consider to be representative for the dots in the ensemble. Since the experiments on the ensemble of QDs average the finer details present in single QDs, we assume disk-shaped QDs. Next, we take into account the known fact of how the fluctuation of the dots height and lateral size depend on the interdot distances, so that for small interdot distances lateral dot size fluctuations are more important (samples D and C from Ref. 18, and sample A from Ref. 19), and for larger interdot distances, when dots behave "more independent" (sample B from Ref. 18) fluctuation of the height of the dots is more pronounced. Thus in order to compare our theoretical findings for the exciton diamagnetic shift for double and triple QDM to the experimental results for small interdot distances $d=2$ and 4 nm (samples D and C from Ref. 18 for triple QDM and sample A from Ref. 19 for double QDM) our QDM representative of the ensemble consists of three or two identical QDs of radius $R=10$ nm, height $h=2$ nm, and in the case of larger interdot distance $d=8$ nm (sample B from Ref. 18) our QDM consists of three identical QDs of radius $R=8$ nm, and height $h=3$ nm. The most pronounced discrepancy between our results and the experimental data is found for interdot distance $d=4$ nm. We attribute this to a dominant influence of the strain between the dots (see discussion in the previous section). For the interdot distance $d=2$ nm as well as for interdot distance $d=8$ nm, a good agreement is achieved.

Figure 10(b) shows the result for the exciton diamagnetic shift of the lowest exciton levels for a triple QDM with in-

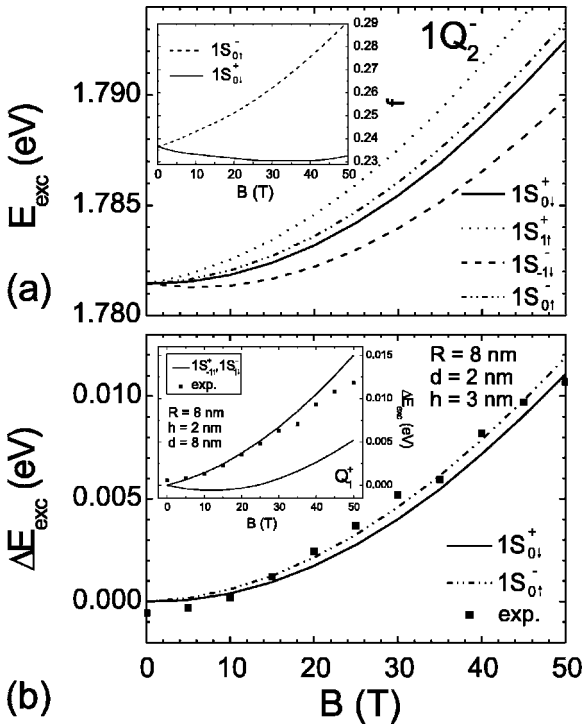

FIG. 12. The same as Fig. 10 but for a dot radius $R=8$ nm, thickness $h=3$ nm, and interdot distance $d=8$ nm.

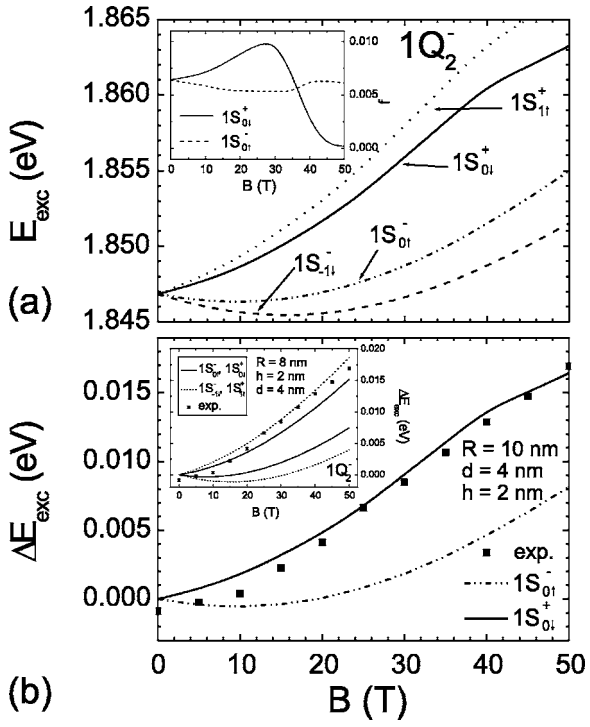

FIG. 13. The same as Fig. 11 but now for a double QDM.

terdot distance $d=2$ nm. The behavior of the individual exciton states of the lowest quartet, in this case the Q_2^- quartet, as a function of the magnetic field is depicted in Fig. 10(a) where in the inset of the figure we show the oscillator strength for the states $S_{0\downarrow}^+$ and $S_{0\uparrow}^-$ of the Q_2^- quartet. All exciton states of the Q_2^- quartet are optically active. However, for x and y light polarization ($S_{+1\uparrow}^+$ and $S_{-1\downarrow}^-$ of the Q_2^- quartet) the oscillator strength (not shown) is approximately 10% of the oscillator strength for z light polarization ($S_{0\downarrow}^+$ and $S_{0\uparrow}^-$ of the Q_2^- quartet). A good agreement between the experimental data and the optically active $S_{0\downarrow}^+$ and $S_{0\uparrow}^-$ states of the Q_2^- exciton quartet are found. As diamagnetic shift carries information about the lateral confinement and the Coulomb interaction, increasing the dot radius in our model decreases the lateral confinement in our dots and increases the influence of the magnetic field. One can see from the inset of Fig. 10(a) that the oscillator strength of the $S_{0\downarrow}^+$ state tends to zero for magnetic fields above 40 T, while the oscillator strength of $S_{0\uparrow}^-$ just slightly decreases with increasing magnetic field. It is easy to see from Fig. 10(b) that the experimental data fits best the $S_{0\uparrow}^-$ state, but the difference between the $S_{0\uparrow}^-$ and $S_{0\downarrow}^+$ energies are small and are within the experimental accuracy of a photoluminescence experiment on an ensemble of QDM. For completeness, the diamagnetic shift of the optically active exciton low-lying quartet where the nominal experimental parameters are used ($R=8$ nm, $h=2$ nm, and $d=2$ nm) is compared to the experimental data in the inset of Fig. 10(b). Even in that case, experimental data are described by the lowest lying exciton quartet.

With increasing distance between the dots we actually decrease the quantum mechanical coupling, as well as the influence of strain on the confinement in the dot. It is, however, known that the strain decays more slowly (with power law) than the electron and hole wave function (exponential decay), and thus strain will dominantly influence the carrier localization and the exciton diamagnetic shift for this interdot distance. Figure 11(a) shows the individual exciton states of the lowest quartet, in this case the Q_1^+ quartet, as a function of the magnetic field. As in the case of interdot distance $d=2$ nm, for $d=4$ nm, the radius of the dots is taken to be 10 nm and height of the dots is 2 nm. In the inset of the figure we show the oscillator strength for the states $S_{-1\downarrow}^+$ and $S_{1\uparrow}^-$ of the Q_1^+ quartet. The other two exciton states $S_{-2\downarrow}^+$ and $S_{2\uparrow}^-$ of the Q_1^+ quartet are dark. The exciton diamagnetic shift in the case of the triple QDM, for interdot distances of 4 nm, is compared in Fig. 11(b) with the experimental data.

As in the case of interdot distance 2 nm, the experimental data are described by the optically active states belonging to the lowest lying exciton quartet. However, the experimental curve fits the exciton state $S_{1\uparrow}^-$ which lies above the optically active state $S_{-1\downarrow}^+$. If one looks at the oscillator strengths in the inset of Fig. 11(a), the oscillator strength of $S_{1\uparrow}^-$ tends to zero for values of magnetic field larger than 40 T, while the oscillator strength of $S_{1\uparrow}^-$ increases with magnetic field. Thus it is questionable that the experimental data are described by the state $S_{1\uparrow}^-$ and the agreement is probably coincidental. As was already pointed out, for the considered interdot distance 4 nm, the dots are mainly coupled by strain. On the other hand, the strain field is very sensitive to the dot size and shape and we assumed in our model three identical vertically aligned disklike quantum dots. Note that the same model has been employed to study the exciton diamagnetic shift in a single InP/InGaP QD,[23] and when comparing with experiment a good agreement was found for a dot height of 2.55 nm and radius 8 nm. Thus our assumption of disklike

quantum dots is justified. However, following the mechanism of growth of a quantum dot molecule, where a pronounced minimum in the elastic strain energy at the surface directly above the dot leads to the preferential growth of a second layer of dots vertically aligned with the first and further to the vertically aligned third layer, modifies the strain distribution in and around dots and directly affects the effective confinement potentials for carriers. Because of the difference in strain fields in the top and bottom dots, it is not likely that the quantum dots in the QDM are identical. It is therefore possible that the exciton is mainly localized in the largest quantum dot. A more precise study should include the yet unknown dot size variation in the stack of dots. As in the case of interdot distance $d=2$ nm, in the inset of Fig. 11(b) we show the diamagnetic shift of the optically active exciton low-lying quartet were the nominal experimental parameters are used ($R=8$ nm, $h=2$ nm, and $d=4$ nm) as compared to the experimental data.

With a further increase of the interdot distance from $d=4$ to 8 nm, coupling due to strain decreases as well. The ground state exciton quartet for the triple QDM in this case is Q_2^-, and it is shown in Fig. 12(a). In the inset of Fig. 12(a) the oscillator strength for the states $S_{0\downarrow}^+$ and $S_{0\uparrow}^-$ of the Q_2^- quartet are shown. As in the case of interdot distance $d=2$ nm, for x,y light polarization ($S_{+1\uparrow}^+$ and $S_{-1\downarrow}^-$ of Q_2^- quartet) the oscillator strength (not shown) is approximately 10% of the oscillator strength for z light polarization ($S_{0\downarrow}^+$ and $S_{0\uparrow}^-$ of Q_2^- quartet). In Fig. 12(b), a comparison between our findings and the experimental ones [Fig. 12(b)] is shown for dot radius $R=8$ nm, height $h=3$ nm, and interdot distance $d=8$ nm. One can see that the experimental data fit the exciton state $S_{0\downarrow}^+$ as well as $S_{0\uparrow}^-$. The difference between the two curves is too small to be discriminated experimentally and we may conclude that there is good agreement between our theoretical results and the experimental data. For completeness, the diamagnetic shift of the optically active exciton low-lying quartet where the nominal experimental parameters are used ($R=8$ nm, $h=2$ nm, and $d=8$ nm) is compared to the experimental data in the inset of Fig. 12(b).

Let us also briefly discuss the results for a double QDM. The ground state exciton quartet is Q_2^- and it is shown in Fig. 13(a) for dot radius $R=10$ nm, thickness $h=2$ nm, and interdot distance $d=4$ nm. Oscillator strength for the exciton recombination for z light polarization is shown in the inset of Fig. 13(a). The exciton diamagnetic shift calculated from our model is compared with the experimental data in Fig. 13(b). In the inset of Fig. 13(b) we show the diamagnetic shift of the optically active exciton low-lying quartet where nominal experimental parameters are used ($R=8$ nm, $h=2$ nm, and $d=4$ nm). From Fig. 13(b) one can see that the experimental data fit the upper lying exciton $S_{0\downarrow}^+$, for which the oscillator strength tends to zero for a magnetic field higher that 40 T [see inset of Fig. 13(a)]. This is the same discrepancy as was found for the triple QDM when the interdot distance is $d=4$ nm (see Fig. 11). We have no clear explanation for this interchange of exciton levels.

IV. SUMMARY AND CONCLUSIONS

Sizes of the dots in the molecule and interdot distance determine whether the hole in the InP/InGaP QDMs sits in the dots, in between the dots, or in the matrix near the bases of the stack. We found that for small interdot distance (<3 nm) the hole settles in the matrix near the bases of the stack or in the dots, while for larger interdot distances the hole can be localized in between the dots or in the dots depending on the dot size. Whenever for $B=0$ T the hole ground state is heavy-hole-like the magnetic field is unable to induce a transition of the hole ground state.

The size of the dots in the molecule and the interdot distance determine which one of the exciton quartets will have the lowest energy and which one of the individual states in the quartet will be the ground state in the presence of an external magnetic field.

Our theoretical findings for the exciton diamagnetic shift for triple and double QDM are compared with the experimental results on the position of the photoluminescence peak. Interdot distance determines whether quantum mechanical coupling (electron-hole overlap) or strain dominantly affect the exciton diamagnetic shift. For small interdot distance (<3 nm) quantum mechanical coupling is the dominant effect and the calculated diamagnetic shift shows good agreement with the experiment. With increasing interdot distance (~ 4 nm) strain instead of quantum mechanical coupling affects dominantly the exciton diamagnetic shift, and experimental data does not fit the lowest lying optically active individual exciton state, but the higher one, which also belongs to the lowest exciton quartet. A similar discrepancy was found for the double QDM with interdot distance $d=4$ nm. Furthermore, for triple QDM with interdot distance $d=8$ nm the dots act "more independently" and the calculated exciton diamagnetic shift shows good agreement with the experiment data.

ACKNOWLEDGMENTS

This work was supported by the Belgian Science Policy, the European Union Network of Excellence: SANDiE, and the Ministry of Science of Serbia.

*Electronic address: vladan.mlinar@ua.ac.be
†Electronic address: francois.peeters@ua.ac.be

[1] G. Schedelbeck, W. Wegscheider, M. Bichler, and G. Abstreiter, Science **278**, 1792 (1997).
[2] M. Bayer, P. Hawrylak, K. Hinzer, S. Fafard, M. Korkusinski, Z. R. Wasilewski, O. Stern, and A. Forchel, Science **291**, 451 (2001).
[3] M. Colloci, A. Vinattieri, L. Lippi, F. Bogani, M. Rosa-Clot, S. Taddei, A. Bosacchi, S. Franchi, and P. Frigeri, Appl. Phys. Lett. **74**, 564 (1999).
[4] E. Biolatti, R. C. Iotti, P. Zanardi, and Fausto Rossi, Phys. Rev. Lett. **85**, 5647 (2000).

[5] P. Borri, W. Langbein, U. Woggon, M. Schwab, M. Bayer, S. Fafard, Z. Wasilewski, and P. Hawrylak, Phys. Rev. Lett. **91**, 267401 (2003).
[6] H. Heidemeyer, U. Denker, C. Müller, and O. G. Schmidt, Phys. Rev. Lett. **91**, 196103 (2003).
[7] Q. Xie, A. Madhukar, P. Chen, and N. P. Kobayashi, Phys. Rev. Lett. **75**, 2542 (1995).
[8] R. Heitz, A. Kalburge, Q. Xie, M. Grundmann, P. Chen, A. Hoffmann, A. Madhukar, and D. Bimberg, Phys. Rev. B **57**, 9050 (1998).
[9] B. Partoens and F. M. Peeters, Phys. Rev. Lett. **84**, 4433 (2000).
[10] L. P. Kouwenhoven, D. G. Austing, and S. Tarucha, Rep. Prog. Phys. **64**, 701 (2001).
[11] G. W. Bryant, Phys. Rev. B **48**, 8024 (1993).
[12] A. Schliwa, O. Stier, R. Heitz, M. Grundmann, and D. Bimberg, Phys. Status Solidi B **224**, 405 (2001).
[13] Weidong Sheng and Jean-Pierre Leburton, Appl. Phys. Lett. **81**, 4449 (2002).
[14] S. Bednarek, T. Chwiej, J. Adamowski, and B. Szafran, Phys. Rev. B **67**, 205316 (2003).
[15] K. L. Janssens, B. Partoens, and F. M. Peeters, Phys. Rev. B **69**, 235320 (2004).
[16] M. Tadić and F. M. Peeters, Phys. Rev. B **70**, 195302 (2004); J. Phys.: Condens. Matter **16**, 8633 (2004).
[17] K. L. Janssens, B. Partoens, and F. M. Peeters, Phys. Rev. B **67**, 235325 (2003).
[18] M. Hayne, R. Provoost, M. K. Zundel, Y. M. Manz, K. Eberl, and V. V. Moshchalkov, Phys. Rev. B **62**, 10324 (2000).
[19] M. Hayne, J. Maes, Y. M. Manz, O. G. Schmidt, K. Eberl, and V. V. Moshchalkov, Appl. Phys. Lett. **79**, 45 (2001).
[20] Q. M. K. Zundel, N. Y. Jin-Phillipp, G. Phillipp, K. Eberl, T. Riedl, E. Fehrenbacher, and A. Hangleiter, Appl. Phys. Lett. **73**, 1784 (1998).
[21] C. Pryor, M. E. Pistol, and L. Samuelson, Phys. Rev. B **56**, 10404 (1997).
[22] M. Tadić, F. M. Peeters, and K. L. Janssens, Phys. Rev. B **65**, 165333 (2002).
[23] M. Tadić, V. Mlinar, and F. M. Peeters, Physica E (Amsterdam) **26**, 212 (2005).
[24] C. R. Pidgeon and R. N. Brown, Phys. Rev. **146**, 575 (1966).
[25] The low-lying states in the quantum dots are not significantly affected by the wetting layer.
[26] C. Pryor, J. Kim, L. W. Wang, A. J. Williamson, and A. Zunger, J. Appl. Phys. **83**, 2548 (1998).
[27] F. B. Pedersen and Y. C. Chang, Phys. Rev. B **53**, 1507 (1996).
[28] F. B. Pedersen and Y. C. Chang, Phys. Rev. B **55**, 4580 (1997).
[29] J. M. Luttinger, Phys. Rev. **102**, 1030 (1956).
[30] V. Mlinar, M. Tadić, B. Partoens, and F. M. Peeters, Phys. Rev. B **71**, 205305 (2005).
[31] I. Vurgaftman, J. R. Meyer, and L. R. Ram-Mohan, J. Appl. Phys. **89**, 5815 (2001).
[32] M. K. Zundel, P. Specht, K. Eberl, N. Y. Jin-Phillipp, and F. Phillipp, Appl. Phys. Lett. **71**, 2972 (1997).